Review

For reprint orders, please contact: reprints@futuremedicine.com

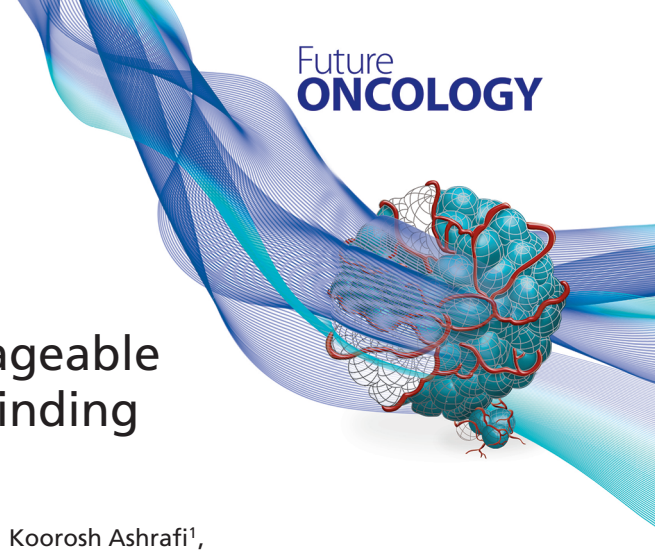

Bench-to-clinic development of imageable drug-eluting embolization beads: finding the balance

Andrew L Lewis*[,1], Sean L Willis[1], Matthew R Dreher[1], Yiqing Tang[1], Koorosh Ashrafi[1], Bradford J Wood[2], Elliot B Levy[2], Karun V Sharma[3], Ayele H Negussie[2] & Andrew S Mikhail[2]

[1]Biocompatibles UK Ltd, a BTG International Group Company, Lakeview, Riverside Way, Watchmoor Park, Camberley, Surrey, GU15 3YL, UK

[2]Center for Interventional Oncology, Radiology & Imaging Sciences, NIH Clinical Center, National Institute of Biomedical Imaging & Bioengineering, & National Cancer Institute Center for Cancer Research, NIH, 10 Center Drive, Bethesda, MD 20892, USA

[3]Department of Radiology & Sheikh Zayed Institute for Pediatric Surgical Innovation, Children's National Medical Center, Washington, DC 20010, USA

*Author for correspondence: Tel.: +44 1276 902204; andrew.lewis@btgplc.com

This review describes the historical development of an imageable spherical embolic agent and focuses on work performed in collaboration between Biocompatibles UK Ltd (a BTG International group company) and the NIH to demonstrate radiopaque bead utility and bring a commercial offering to market that meets a clinical need. Various chemistries have been investigated and multiple prototypes evaluated in search of an optimized product with the right balance of handling and imaging properties. Herein, we describe the steps taken in the development of DC Bead LUMI™, the first commercially available radiopaque drug-eluting bead, ultimately leading to the first human experience of this novel embolic agent in the treatment of liver tumors.

Graphical abstract:

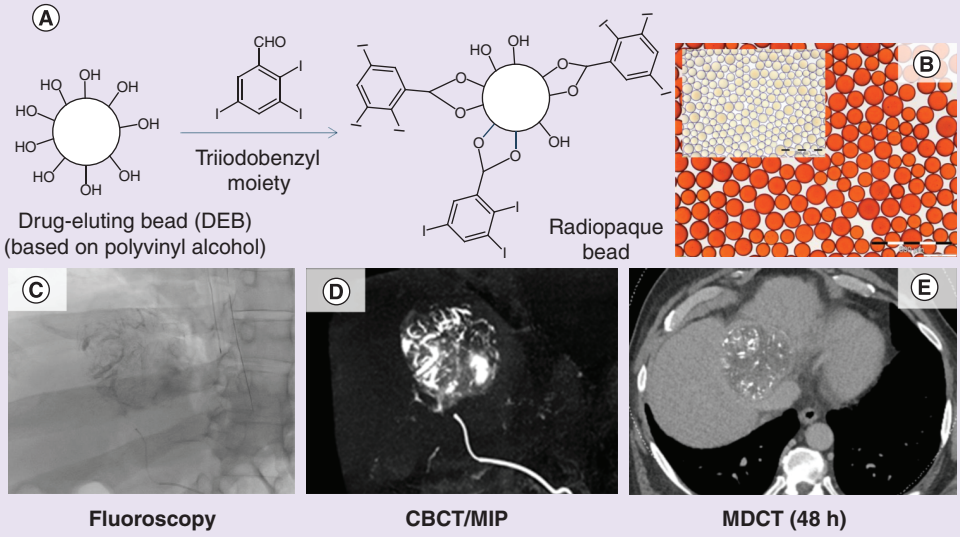

(A) Method of radiopaque bead (ROB) preparation

(B) Unloaded ROB (inset) and doxorubicin loaded ROB

(C–E) Flouroscopy, CBCT MIP immediately post-procedure and MDCT image at 48 h of a human hepatocellular carcinoma tumor containing ROB

First draft submitted: 14 March 2018; Accepted for publication: 24 May 2018; Published online: 26 June 2018

Future Medicine

Keywords: cone-beam computed tomography • drug-eluting bead • radiopacity • radiopaque bead • transarterial chemoembolization

Transarterial embolization is the intentional occlusion of a blood vessel by introduction of an agent via a catheter placed within the vasculature that creates a blockade to further blood flow. Embolization agents come in many forms and can include devices such as balloons and coils, liquids such as glue, gelling polymer solutions and sclerosing agents such as alcohol, or most commonly particles or microspherical embolics made from hydrogels [1–3]. Many of the commercially available embolic materials are colored with dyes in order to make them easier to see during handling and administration but they are difficult to detect during and after administration because they are not directly visible under standard x-ray, magnetic resonance (MR), ultrasound or nuclear medicine imaging techniques.

There exists, however, a genuine clinical need for embolic agents that can provide intraprocedural and postprocedural feedback with standard imaging techniques, in order to permit the interventionalist to optimize treatment technique and hence potentially improve clinical outcomes [4]. The ability to directly see where the beads are going may enable the physician to more precisely target the area of treatment, detect and standardize end points more appropriately [5,6], identify areas of potential undertreatment during the procedure and potentially improve patient safety by detecting off-target embolization [7]. There has been a recent interest in the development of imageable embolization agents, largely driven by advancements in imaging techniques that now make detection easier and more informative; but it is fair to say that this is not a new concept. The inclusion of heavy elements into the embolic agent structure in order to increase electron density and hence ability to absorb x-rays has been investigated for many years with mixed success (Table 1). The ability to visualize the embolic agent under x-ray imaging usually comes at a cost, namely the increase in density of the product, which can make the handling and administration properties of the product challenging.

Multiple experimental efforts to develop imageable particulate embolic agents are reported in the literature (Table 1). In some cases, the particulates have been rendered radiodense by the incorporation of metallic components such as barium (Figure 1A) [9,11,13] or tantalum (Figure 1C & D) [12,29]. Barium sulfate powder inclusion or salt precipitation within the particle has been shown to affect both the internal and surface morphologies, often resulting in roughness and porosity that was thought desirable for thrombus formation and tissue integration [11]. On the other hand, polyurethane or silicone particulates with substantially smooth surfaces have been rendered radiopaque by inclusion of tantalum powder, but shown to possess hydrophobic surfaces that hinder microcatheter delivery without surface treatments such as grafting with hydrophilic compounds [12,29]. Both approaches can have adverse effects on the handling and administration of the embolic agent, with increased particle density inducing rapid sedimentation and increasing the likelihood of catheter blockage [30].

The incorporation of iodine-containing species into polymers has been a more widely studied approach, resulting in biomaterials useful in tissue bulking applications [32], orthopedic bone cements [33,34], vertebral disc repair [35,36] and as embolic microparticles [8,37]. The radiopacity can be introduced by: (1) the chemical attachment of a reactively functional iodinated species to preformed polymer particles [8,27,28]; (2) the inclusion of an iodine-bearing monomer during the particle polymerization stage [14,15,37]; (3) or by entrapment of an iodine-containing compound within the particle structure [13,24,31]. Whatever the approach, compounds consisting of iodinated benzyl groups (as found in most commercial x-ray contrast agents) are commonly employed as they offer synthetic flexibility and enable incorporation of high iodine contents per unit mass, which improves conspicuity. Using approach (1), radiopaque microparticles have been readily prepared by attachment of 2,3,5-triiodobenzyl (TIB) moieties [8], but while iodine contents in the 25–30 weight% region were possible, the hydrophilicity and softness attributes that are desirable for the handling and microcatheter delivery of embolization beads were adversely compromised. One proposed solution was approach (2) involving the copolymerization of TIB-based monomers such as 3-(methacryloylamidoacetamido)-2,4,6-triiodobenzoic acid with hydrophilic comonomers like hydroxyethyl methacrylate in the presence of additives to induce porosity to the microspheres (Figure 1B) [14]. It was found that a minimum of 27 weight% iodine was required for adequate radiopacity but resulted in irregular particle formation and agglomeration during the polymerization. An alternative approach to increasing the hydrophilicity was to use the less hydrophobic mono-iodinated 2-[4-iodobenzoyl]-oxo-ethylmethacrylate monomer (Figure 1E) copolymerized with hydrophilic comonomers such as hydroxyethyl methacrylate or 1-vinyl-2-pyrrolidinone [15]. This resulted in microparticle formulations that were water-absorbent in nature but only those with low water content and iodine contents of approximately 20 weight% were sufficiently radiopaque to be useful in practice. Using approach (3), radiopaque

Table 1. Selection of imageable embolic microsphere systems described in the literature.

Embolic agent matrix	Imaging component	Method of inclusion	Imaging modality	Comments	Study (year)	Ref.
PHEMA	Iodine (triiodobenzyl groups)	Covalent coupling	X-ray	25–30 wt% loading	Horak *et al.* (1987)	[8]
PMMA (hydrolyzed)	Barium sulfate	Precipitation	X-ray	70 wt% loading achieved	Thanoo and Jayakrishnan (1989)	[9]
PHEMA	Iodine (iothalamic/iopanoic acid)	Covalent esterification	X-ray	30 wt% loading achieved	Jayakrishnan *et al.* (1990)	[10]
PHEMA	Barium sulfate	Entrapment	X-ray	40–50 wt% loading achieved	Thanoo and Jayakrishnan (1990)	[11]
Silicone	Tantalum powder	Entrapment	X-ray	Needed surface modn.	Thanoo and Jayakrishnan (1991)	[12]
Polyurethane	Tantalum powder	Entrapment	X-ray	Needed surface modn.	Thanoo *et al.* (1991)	[13]
PHEMA copolymer	Iodine (triiodobenzyl monomer)	Copolymerization	X-ray	27 wt% achieved	Horak *et al.* (1997)	[14]
PHEMA/PVP copolymers	Iodine (monoiodobenzyl monomer)	Copolymerization	X-ray	20 wt% achieved	van Hooy-Corstjens *et al.* (2008)	[15]
Trisacryl (embosphere)	Iron oxide (SPIO)	Entrapment	MR	Detectable by common echo sequences	Namur *et al.* (2007)	[16]
Trisacryl (embosphere)	Iron oxide (SPIO)	Entrapment	MR	100% detectable	Lee *et al.* (2008)	[17]
Alginate	Holmium	Complexation	MR/gamma	1.3 wt% Ho loading	Zielhuis *et al.* (2007)	[18]
PVA	Gadolinium III Chelates	Covalent coupling	MR	45.5 μg Gd(III)/mg PVA	Cilliers *et al.* (2008)	[19]
Alginate	Holmium and iodine (Lipiodol®)	Complexation/entrapment	CBCT/MR	0.38% Ho loading	Oerlmans *et al.* (2015)	[20]
Alginate	Barium sulfate	Complexation	DSA/CT	Microfluidic method	Wang *et al.* (2015)	[21]
Chitosan	Iron oxide (SPIO)	Entrapment	MR	1.0 mM SPIO loading	Chung *et al.* (2012)	[22]
PMAA (embozene)	Barium sulfate/iodine/iron oxide	Precipitation/entrapment	Radiography/MR/CT	Three different loading densities	Stampfl *et al.* (2012)	[23]
PVA-AMPS (DC/LC bead)	Iodine (Lipiodol)	Entrapment	Fluoro/μCT/CT	Dose-dependent imaging	Sharma *et al.* (2010)	[24]
PVA-AMPS (DC/LC bead)	Iodine (Lipiodol)	Entrapment	Fluoro/μCT/CT	Correlation with drug	Dreher *et al.* (2012)	[25]
PVA-AMPS (DC/LC bead)	Iodine (Lipiodol)	Entrapment	Fluoro/μCT/MDCT/CBCT	Different imaging modes	Tacher *et al.* (2016)	[26]
PVA-AMPS (DC/LC bead)	Iodine (triiodobenzyl groups)	Covalent attachment	μCT/CT	Drug loading demonstrated	Negussie *et al.* (2015)	[27]
PVA-AMPS (DC/LC bead)	Iodine (triiodobenzyl groups)	Covalent attachment	Fluoro/μCT/CT	IR imaging reading study	Duran *et al.* (2016)	[28]

CBCT: Cone-beam computed tomography; CT: Computed tomography; DSA: Digital subtraction angiography; Ho: Holmium; modn: Modification; MDCT: Multidetector computed tomography; MR: Magnetic resonance; PHEMA: Poly(2-hydroxyethyl methacrylate); PMMA: Poly(methylmethacrylate); PVP: Poly(N-vinyl-2-Pyrrolidone); PMAA: Poly(methylacrylic acid); PVA-AMPS: Poly(vinyl alcohol-co-2-acrylamido-2-methylpropane sulfonate); SPIO: Super paramagnetic iron oxide.

compounds can be incorporated into the particle matrix (Figure 1F) [13,31], but here it is important that the compounds rendering radiopacity remain entrapped and do not leach out over time.

These studies clearly demonstrate the fine balance that exists between the need for sufficient x-ray density for good imageability while maintaining appropriate physicochemical properties that will allow for the practicalities of microparticle administration. Many of the approaches described in the early 1990s aimed to incorporate as much radiodense material as possible to render the agents visible under x-ray, but specific imaging modalities for evaluation were limited. The field went relatively quiet for a decade or so, until the mid-2000s, where the appearance of commercial drug-eluting beads (DEB) [38–42] and the introduction and establishment of cone-beam computed tomography (CBCT) as a mainstream imaging technique to be used during transarterial chemoembolization (TACE) [43–45] reignited interest in the potential for embolic agent imageability. Reports were more comprehensive in the type of imaging method used and indeed, often including use of different imaging modes, with some prototype agents incorporating multiple imaging components to render them imageable under both x-ray- and MR-based methods [20,23,24,26]. Most recently, this has led to the development of 'nano-on-micro' systems in which

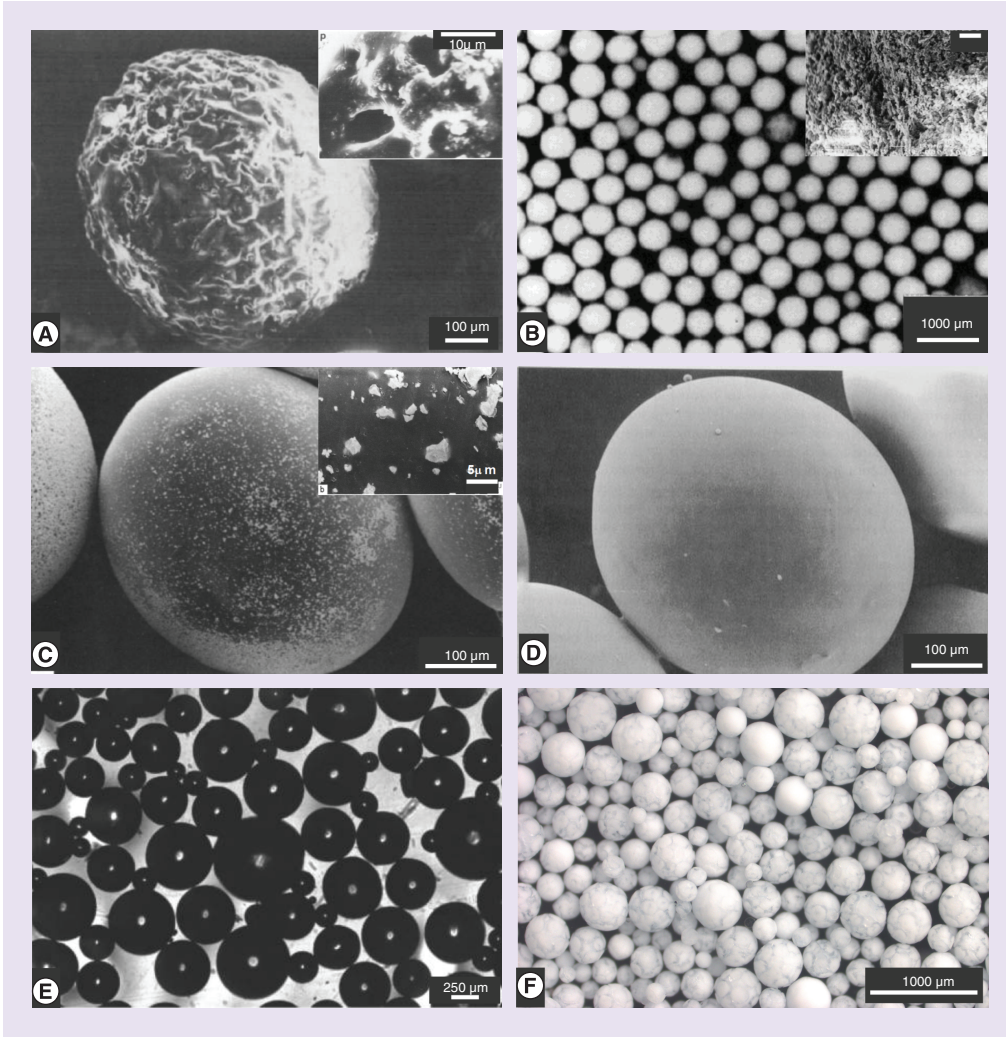

Figure 1. Selected examples of radiopaque embolization microparticle prototypes. (A) Poly(2-hydroxyethyl methacrylate) microparticles incorporating barium sulfate – note the rough surface (inset: porosity can be seen on the magnified surface). **(B)** Microparticles of 3-(Methacryloylamido-acetamido)-2,4,6-triiodobenzoic acid-Hydroxyethyl methacrylate-EDMA copolymer (inset: porosity can be seen on the magnified surface). **(C)** Polyurethane microspheres containing entrapped Ta particulates (see magnified inset for tantalum particle size and shape). **(D)** Silicone microspheres with entrapped tantalum particulates. **(E)** Microspheres made from Hydroxyethyl methacrylate-2-[4-Iodobenzoyl]-oxo-ethylmethacrylate copolymers. **(F)** Poly(vinyl alcohol-co-2-acrylamido-2-methylpropane sulfonate) microspheres containing Lipiodol® (note the marbled appearance of the oil and water phases within the microspheres).
(A) Reproduced with permission from [11] © Elsevier (1990).
(B) Reproduced with permission from [14] © John Wiley & Sons Inc. (1997).
(C) Reproduced with permission from [29] © Elsevier (1991).
(D) Reproduced with permission from [12] © Taylor and Francis (1991).
(E) Reproduced with permission from [15] © American Chemical Society (2008).
(F) Reproduced with permission from [31] © Elsevier (2016).

multifunctionality is introduced into the microparticles by the inclusion of nanoparticles within their matrix [46]. For instance, thermosensitive liposomes containing both a drug and T1 MRI agent have been entrapped within alginate microspheres cross-linked with a T2 imaging agent for enhanced MR imageability [47]. Alternatively, both computed tomography (CT) and MRI capability have been enabled in alginate drug-eluting microspheres by inclusion of radiopaque gold nanorods and magnetic iron clusters using microfluid fabrication techniques [48]. In this review, we describe our motivation and efforts to evolve the concept of imageable beads from the prototype stage with the development and translation of the first commercially available radiopaque DEB.

Current practice of TACE

TACE is a method of intra-arterial locoregional drug delivery combined with embolization, which is currently practiced in two broad forms: conventional oil-based TACE (cTACE) and DEB-TACE [49–54]. While their basic therapeutic concept combines aspects of drug delivery and blood vessel occlusion into one therapeutic procedure that are similar, they have quite distinctly different mechanisms of action [55–59].

In cTACE, an aqueous chemotherapy solution (and often aqueous-based contrast agent) is mixed with Lipiodol (a mixture of monoiodonated esters of poppy seed oil) to form a water-in-oil emulsion. The chemotherapeutic can be a monotherapy of one drug (e.g., doxorubicin or cisplatin) or a mixture of agents (often cisplatin, adriamycin [doxorubicin] and mitomycin – known as CAM) [5]. The emulsion is injected intra-arterially into the blood vessels feeding tumors reducing the blood flow as the emulsion breaks into droplets within the vasculature. The embolization is completed by a second step in which a particulate embolic agent, such as Gelfoam slurry or calibrated microspheres, is injected into the same target vessels to occlude the blood flow completely and retard the washout of the chemotherapeutic from the emulsion droplets and embolized tissue [60].

DEB-TACE was developed in order to simplify and standardize TACE in a one-step procedure by allowing chemotherapeutic to be loaded into the embolic agent prior to administration and subsequently released in a controlled and sustained manner from the embolic beads themselves postembolization in the tumor vessels [42,61,62]. Pharmacokinetic studies in both animals and humans confirm that systemic exposure to the chemotherapy is significantly reduced whereas tumor drug levels are much higher than achieved by cTACE [63–65]. Moreover, there is a significant decrease in the level of liver enzymes post-DEB-TACE compared with cTACE [66], which is consistent with more precise tumor-targeting and less widespread liver injury caused by total liver exposure to the drug (especially early drug bursts).

Aspects of conventional TACE

Lipiodol possesses iodine atoms attached to the fatty chains, which render it radiodense; when a cTACE emulsion is injected into the blood stream, it is clearly visible under standard fluoroscopic imaging and can be monitored flowing into the vascular network where it accumulates to leave a 'blush' of contrast in the target region. The droplets, however, can also penetrate the sinusoids and pass into the portal venous system, exposing more of the liver and systemic circulation to drug, hence potentially increasing the likelihood of liver-related and systemic toxicities [66,67]. The droplets are cleared from normal tissue in approximately 1 week by release from the hepatic sinusoids and phagocytosis by Kupffer cells [68–70]. Follow-up multidetector computed tomography (MDCT) imaging can often appear as a compact, homogeneous deposition of Lipiodol in the tumor, giving the appearance that Lipiodol carries drug and selectively targets the tumor, which is not quite the case [71]. Gaba *et al.* conducted an analysis of the correlation between the location of iodine (Lipiodol) with that of doxorubicin in various sections of a VX2 tumor post-treatment with cTACE emulsion [72]. Unsurprisingly, they found no direct correlation between the drug and oil locations, which further supports the notion that Lipiodol is not the ideal drug-carrying vector and cannot be used to predict drug localization on the basis of imaging appearance of Lipiodol. Nevertheless, the Lipiodol imaging appearance is widely accepted as a predictor of tumor response and evidence of a successful TACE procedure [73], although this is not always predictive [74,75] and indeed, the dense radiopacity can sometimes mask the enhancement of underlying viable tumor [76]. Intraprocedural CBCT has been shown to be as predictive as MDCT, although in many cases the Lipiodol appears diffuse throughout the liver as it has not had time to be cleared from the entirety of the healthy liver [77]; Despite this, comparison of Lipiodol retention pattern by CBCT is more predictive of short-term response than by use of fluoroscopy [78] and moreover, 3D quantification of Lipiodol deposition by CBCT has been shown to correlate to tumor response on contrast-enhanced MRI follow-up [79].

Aspects of DEB-TACE

There are several commercially available DEBs on the market, all of which are currently based upon water-swollen hydrogel microspheres. Their water-swollen nature and calibrated sizes allow them to be delivered through microcatheters to target particular vascular dimensions. Their size and physical compressibility prevent passage into the portal venous system or hepatic veins, notwithstanding the presence of a sufficiently large shunt. The process of embolization is dynamic, with some vessels opening as others are closed due to redirection of flow [80]. With DEB, it is the rate of contrast agent clearance from the target vessel that is used as a treatment endpoint and it is thought that best outcomes are achieved with the observation of near complete flow stasis rather than with total vessel

occlusion [81]. At this point, digital subtraction angiography clearly shows the areas that have been devascularized by the beads, the aim being extinction of tumor-related contrast blush. However, as DEBs are radiolucent, they are invisible under x-ray imaging and downstream location can only be inferred from static vessels. More recently, it has been observed that by use of CBCT postembolization with DEB, a pattern of retained contrast agent that is trapped by the embolization may be observed [82,83]. This is best imaged immediately, but may persist for some hours before fading as the contrast washes out. This pattern of trapped contrast on CBCT has been shown to be useful for predicting tumor response, but again, the exact location of the beads (or lack of) is not directly visualized, and hence drug location is not directly visualized. It is, therefore, not easy to appreciate or communicate whether a DEB-TACE procedure has been truly successful until the follow-up imaging reveals the extent of nonenhancement in the treated tumor. For these reasons we have been collaborating for several years on developing ways to make the DEBs radiopaque under conventional x-ray and CBCT-based techniques for enhancing the DEB-TACE procedure.

Feasibility of a radiopaque DEB: get the balance right

Having reviewed the historical literature (Table 1), we initially focused our efforts on methods to entrap either iodine (in the form of Lipiodol) into lyophilized beads or barium sulfate precipitation into the hydrated bead matrix in order to make prototypes that we could use to evaluate the utility of embolic particle radiopacity. Our initial attempts indeed yielded beads that could be imaged under CT with acceptable levels of radiopacity with either approach (Figure 2). The first-generation barium beads were prepared according to the method described by Thanoo and Jayakrishnan [9] and were found to be extremely difficult to handle and sediment with gravity extremely quickly. Figure 2C is an optical micrograph that shows the precipitated barium sulfate particles entrapped within the hydrogel polymer microsphere matrix. The second generation overcame these issues but at the cost of a much reduced radiopacity that was considered insufficient for adequate visibility (Figure 2D & E). We turned our focus to the process of Lipiodol incorporation into lyophilized beads, which involved soaking the dry beads in Lipiodol, followed by removal of excess Lipiodol via subsequent washes with ethanol, and finally water to hydrate the beads. The aim was to incorporate high levels of oil with much lower residual levels of free Lipiodol present external to the beads. The oil and water phases that exist within the internal structure of these hydrated microspheres can clearly be seen both optically and by micro-CT analysis (Figure 2A & B, respectively). Our optimized prototype using this approach yielded an ideal product that allowed us to move into *in vivo* feasibility evaluations [31].

Using a rabbit VX2 tumor model, we were able to compare the distribution of the radiopaque DEBs of different size ranges to that of a Lipiodol emulsion administered into the same feeding arteries, by scanning the treated lobes *ex vivo*. Figure 3 shows the comparative CT and micro-CT images. Clearly, beads distribute into arteries according to their size and can therefore be targeted precisely. The larger 100–300 μm beads accumulated more proximally in the larger hepatic arteries located more centrally in the rabbit liver lobe, the 70–150 μm beads occluded more distally, mostly mid-lobe but almost reaching the liver capsule surface, whereas the 30–70 μm beads were most distal of all, filling small vessels at the periphery of the lobe. Micro-CT was able to visualize to single-bead resolution, showing trains of single larger beads stacked in some vessels, or multiple beads packed within the vessel architecture. The appearance of the Lipiodol emulsion was very different. In contrast, there were Lipiodol droplets all around the tumor vascular network and also throughout the lobe, presumably penetrating across the sinusoid connection into the portal system. We have seen the presence of Lipiodol throughout the liver in addition to around the tumor, post a cTACE procedure even at 7 days. The biological half-life of radiolabeled Lipiodol in normal liver has been reported to be 38.5 h [84] but can stay within the tumor indefinitely, as there are no Kupffer cells or lymphatic vessels present in a tumor to eliminate the Lipiodol.

Our initial investigations of the use of radiopaque DEBs were in the embolization of healthy swine liver and kidney models [24]. The beads were visualized during transcatheter embolization with routine intraprocedural fluoroscopy and CT and provided a 3D spatial distribution of embolic material inside target organs constituting real-time intraprocedural feedback for the interventional radiologist. We concluded that the beads may be useful for demonstrating the influence of material and technical variability in transcatheter embolization in addition to providing intraprocedural identification of tissue at risk of undertreatment. It was apparent that the soluble contrast overemphasized the central larger vessels, whereas the radiopaque particles began to localize peripherally, at least early in an embolization.

In our follow-on studies, we then introduced the addition of doxorubicin to the beads (Figure 4A & B) and demonstrated that degree of radiopacity was not only correlated to bead suspension concentration (Figure 4C & D) but that also the measured attenuation of the beads was directly proportional to the concentration of the drug

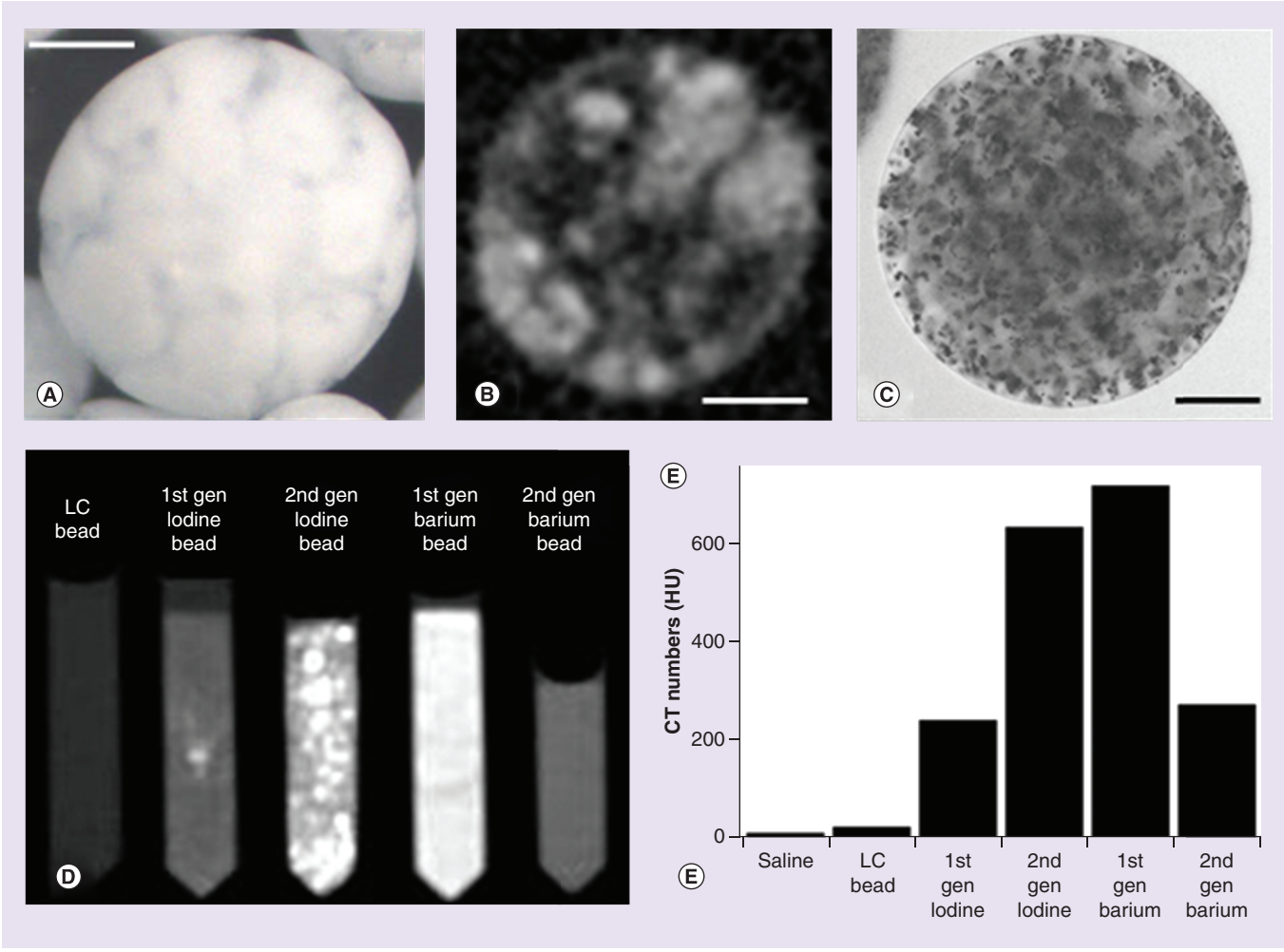

Figure 2. Appearance and properties of early radiopaque bead prototypes. (A) Optical image of Lipiodol-loaded bead. Note the marbled appearance caused by the separation of the oil and water phases within the microsphere structure. **(B)** Micro-CT image of the Lipiodol-loaded bead highlighting the oil (light) and water (dark) phases in the internal structure. **(C)** Optical image of a barium sulfate-loaded bead clearly showing the precipitated barium sulfate particulates within the hydrogel structure. Scale bars are 100 μm for **(A–C)**. **(D)** Beads suspended in tubes imaged with CT shown with window settings chosen to display maximum contrast. **(E)** Corresponding quantitative CT numbers calculated for saline, unloaded LC beads, first generation and second generation of iodine- and barium-loaded beads.
CT: Computed tomography.

present in the adjacent tissue (Figure 4E) [31]. This was the first report of a correlation between image intensity of a radiopaque DEB and its drug content. When imaged *in vivo* we showed that smaller DEBs (70–150 μm) penetrated further into targeted tissue (i.e., macroscopic) with a higher spatial density than larger ones (100–300 μm), resulting in greater and more uniform drug coverage in the targeted normal swine liver. Further studies on these beads administered into a rabbit VX2 tumor model demonstrated that they could be adequately visualized under standard fluoroscopy, x-ray single-snapshot, CBCT, MDCT and micro-CT [26].

Optimization of a radiopaque DEB useful for clinical practice: DC Bead LUMI™

While the Lipiodol-loaded radiopaque bead has been an excellent tool to demonstrate the utility of a radiopaque DEB system, its preparation is complex and impractical for day-to-day clinical use [31]. We set about trying to make an alternative system, again based upon the DC Bead chemistry featuring chemical bonding of the radiopaque component (and hence an inherent part of the particle). Our review of the literature had shown that the materials based on the triiodinated benzyl group chemistry possessed excellent biocompatibility [85] by either *in vitro* cell-based analyses or *in vivo* implantation studies. Our preferred route was to modify the preformed polyvinyl

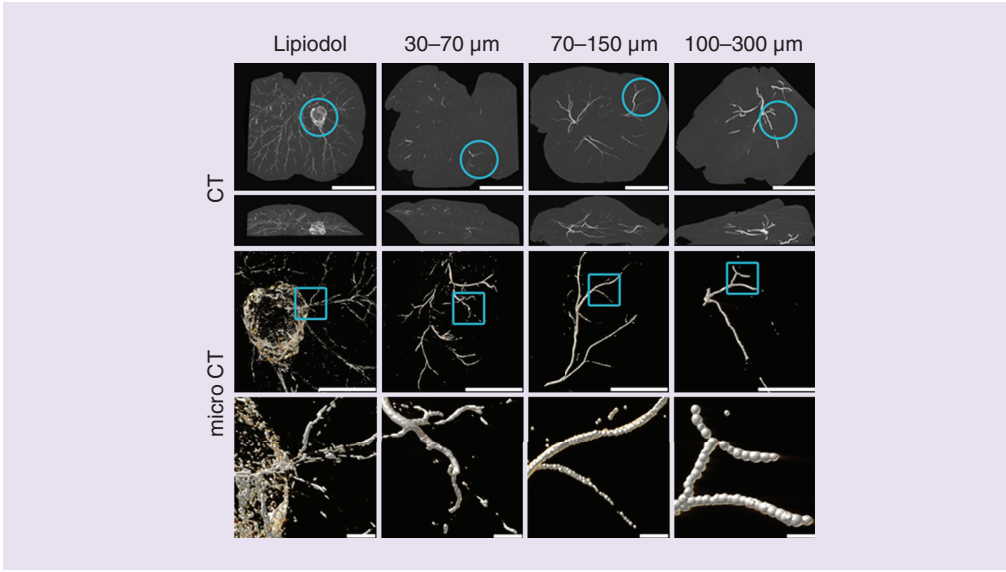

Figure 3. Comparison of computed tomography and micro-computed tomography imaging for rabbit VX2 tumor liver sections treated with intra-arterial administration of either Lipiodol or Lipiodol-loaded beads of various size distributions. Note the smaller the bead, the more distal and peripheral the distribution in the vessels. Lipiodol penetrates the portal venous system whereas beads do not.
CT: Computed tomography.

alcohol-2-acrylamido-2-methylpropane sulfonate (PVA-AMPS)-based hydrogel beads, as modification of the PVA macromer with high iodine levels did not allow for subsequent bead formation. This type of solid-phase reaction has pros and cons: the benefits include being able to start with a largely unchanged bead chemistry; enabling a greater local concentration of reactants within the solid phase, given a suitable solvent is identified; and potentially easier purification and removal of excess reactants or by-products. The downside can be inefficiency of reaction if the linking chemistry is not facile as well as potential inhomogeneity of reaction throughout the bead structure. Indeed, early attempts yielded halo-like effects on bead imaging by micro-CT where reaction was preferential at the surface of the bead but less-so in the central portions (Figure 5).

Our first approach involved activation of the preformed PVA hydrogel bead toward various triiodinated reactants in order to couple radiopaque moieties while maintaining the original hydrogel network structure [27]. Specifically, we favored activating hydroxyl groups on the bead with 1,1′-carbonyldiimidazole followed by attachment of 1,3-diaminopropane as a spacer to alleviate steric hindrance and finally conjugating with 2,3,5-triiodobenzoic acid to impart the radiopacity [27]. The resulting beads were easily seen using x-ray imaging methods, but we discovered that the attachment of the radiopaque groups using a long flexible linker allowed for structural reorganization during sterilization that affected the ability of the beads to load significant amounts of drug.

To overcome this phenomenon, we developed a surprisingly facile approach that involves the direct coupling of TIB groups to the 1,3-diol units of the beads. Dimethyl sulfoxide is used as a reaction solvent that also causes the beads to swell significantly in order that 2,3,5-triiodobenzaldehyde can penetrate the entire bead matrix and react with the 1,3-diol structure of the PVA backbone to form cyclic acetal linkages with the radiopaque moiety (Figure 6A). The uniformity of coupling within single beads and across many beads from multiple batches has been shown by use of energy-dispersive x-ray analysis of physically cross-sectioned beads and by micro-CT imaging analysis of whole beads embedded in agarose phantoms [86]. The process yields beads that are a translucent golden color when hydrated and observed under optical microscopy, indicating that there are no apparent phase-separated domains of the hydrophilic and hydrophobic portions of the structure (Figure 6B). The 2,3,5-triiodobenzaldehyde coupling had to be optimized to obtain the best balance between increase in bead density and subsequent challenges in bead handling and administration versus levels of radiopacity (Figure 6C–E).

The degree to which the beads were visible was evaluated under various modes of imaging performed both *in vitro* and *in vivo*. Suspensions of various bead formulations were subjected to micro-CT to optimize imageability (Figures 6C & D, 7A–C). Line phantoms of different line diameters were made to estimate the size of the vessels that

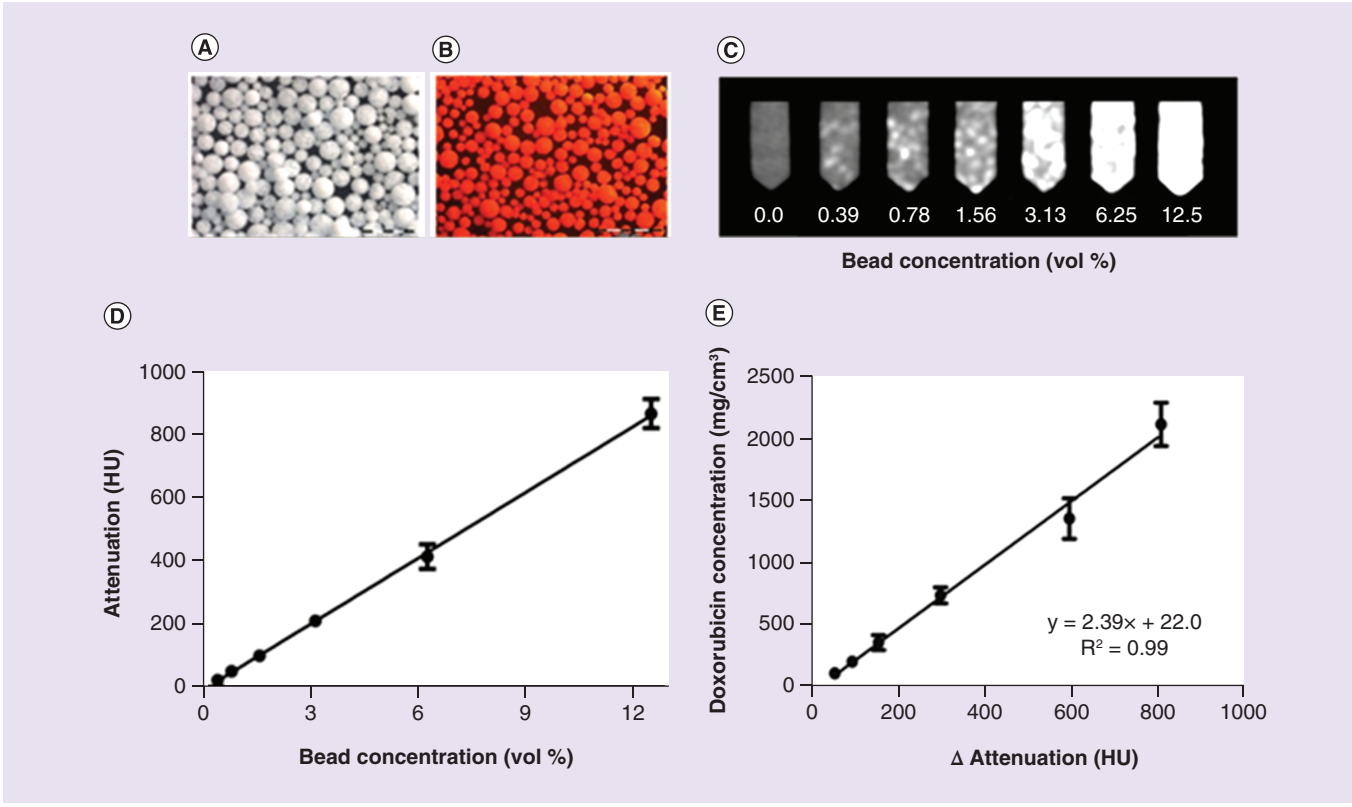

Figure 4. Correlation of bead radiopacity with drug loading. (A) Lipiodol-loaded radiopaque bead; **(B)** doxorubicin/Lipiodol-loaded radiopaque bead (37.5 mg/ml doxorubicin); **(C)** multidetector computed tomography panel of agar phantoms increasing bead concentration in suspension; **(D)** correlation of image attenuation (Hounsfield units) versus bead suspension concentration; **(E)** correlation of doxorubicin concentration in the beads with bead attenuation.
CT: Computed tomography.
Reproduced with permission from [31] © Elsevier (2016).

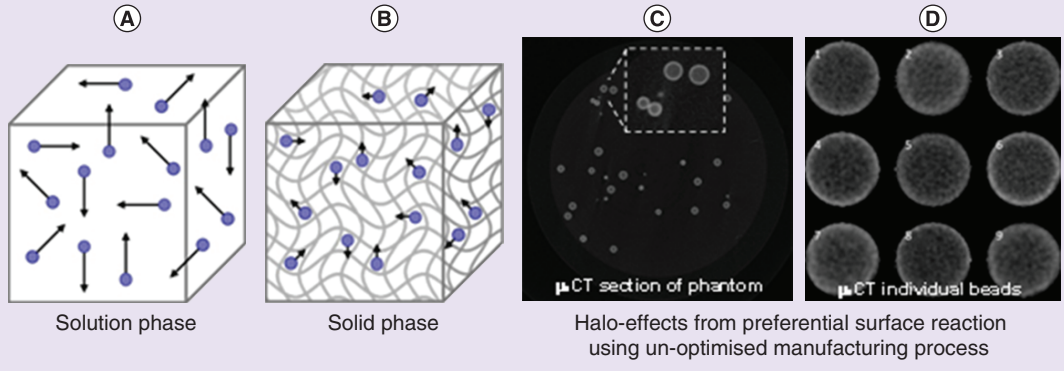

Figure 5. Efficiency of linking reactions. Reactions in solution rely upon diluted reactants coming into contact in order to react **(A)**, whereas in the solid phase the reactants can be concentrated together to aid in coupling efficiency **(B)**. If, however, the reactants cannot penetrate the solid structure completely, an inhomogeneous reaction can occur which can lead to radiopaque groups more prevalent at the surface of the beads and a halo-like image observed by micro-CT **(C & D)**.
CT: Computed tomography.

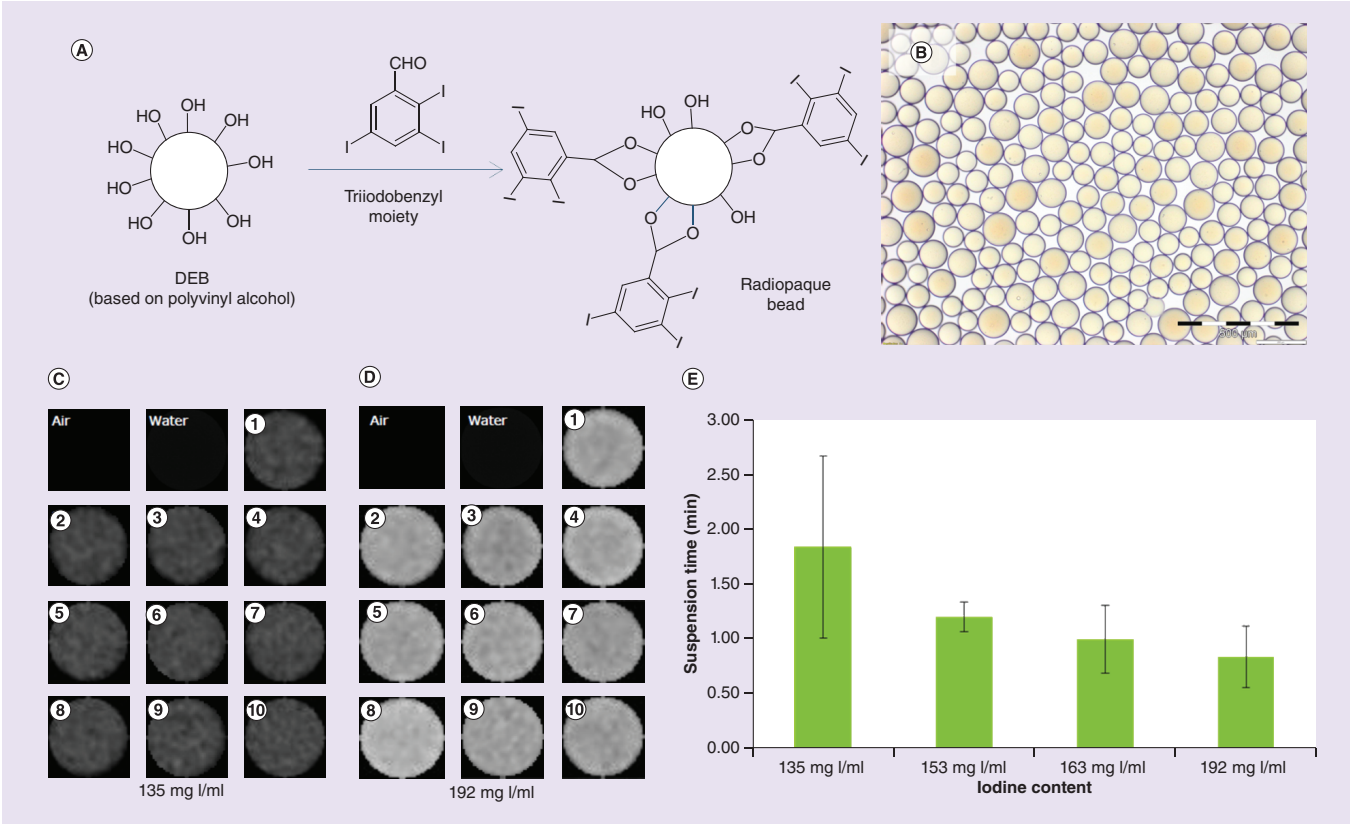

Figure 6. Preparation, appearance and radiopacity of TIBA-based radiopaque beads. Schematic of the coupling of TIBA to PVA-AMPS beads **(A)** and optical micrograph of the 70–150-μm sieved fraction of beads **(B)**. Micro-CT images of ten representative beads made with a target of **(C)** 135 mg I/ml compared with **(D)** 192 mg I/ml and **(E)** their corresponding suspension time in Omnipaque 350® showing how more iodine increases density and promotes rapid sedimentation.
CT: Computed tomography; DEB: Drug-eluting bead; PVA-AMPS: Poly(vinyl alcohol-co-2-acrylamido-2-methylpropane sulfonate); TIBA: Triiodobenzaldehyde.

would be visualized using standard fluoroscopy or single-shot imaging (Figure 7D & E). These tests demonstrated that neither bead size nor drug loading had any impact on the imaging resolution of the beads, only the diameter of the vessel being filled that determines the path length over which the x-ray will be absorbed by the beads appeared to be significant, assuming bead packing densities are similar between sizes [86]. Different bead suspension concentrations were evaluated using MDCT in order to determine where streaking might start to occur at the higher iodine contents (Figure 7F). The optimized system was shown to possess water contents in the region of 60–70% with iodine contents in the range of 189–258 mg/ml true bead volume, equivalent to 46–49 weight% iodine on a dry mass basis (target ~150 mg I/ml of hydrated sedimented beads with reference to Figure 5) [28]. This provided for an excellent degree of radiopacity, while maintaining practical handling benefits. Long-lived bead suspension was found to be best obtained by use of viscous contrast media such as Omnipaque 350® or even better with Visipaque 320®.

Long-term imaging and biocompatibility evaluation was conducted on the optimized 70–150 μm DC Bead LUMI product in a swine hepatic embolization study [87]. This showed that the beads were clearly visible on MDCT, with or without intravenous (iv.) contrast administration (although best imaged without contrast) as the beads are more radiodense than the iv. contrast and appear brighter. The CT imaging appearance was seen to remain consistent over the 90-day study period, indicating that the beads do not degrade or lose any of their radiopacity over time (Figure 8A–D). Embolization was associated with transient elevation of liver enzymes that resolved to baseline within a week and were consistent with the pathological changes in the liver as a consequence of the hepatocellular injury from the ischemic insult (Figure 8E). Histopathological evaluation of tissue sections containing beads showed a classic foreign body response with initial inflammation at the early time points followed

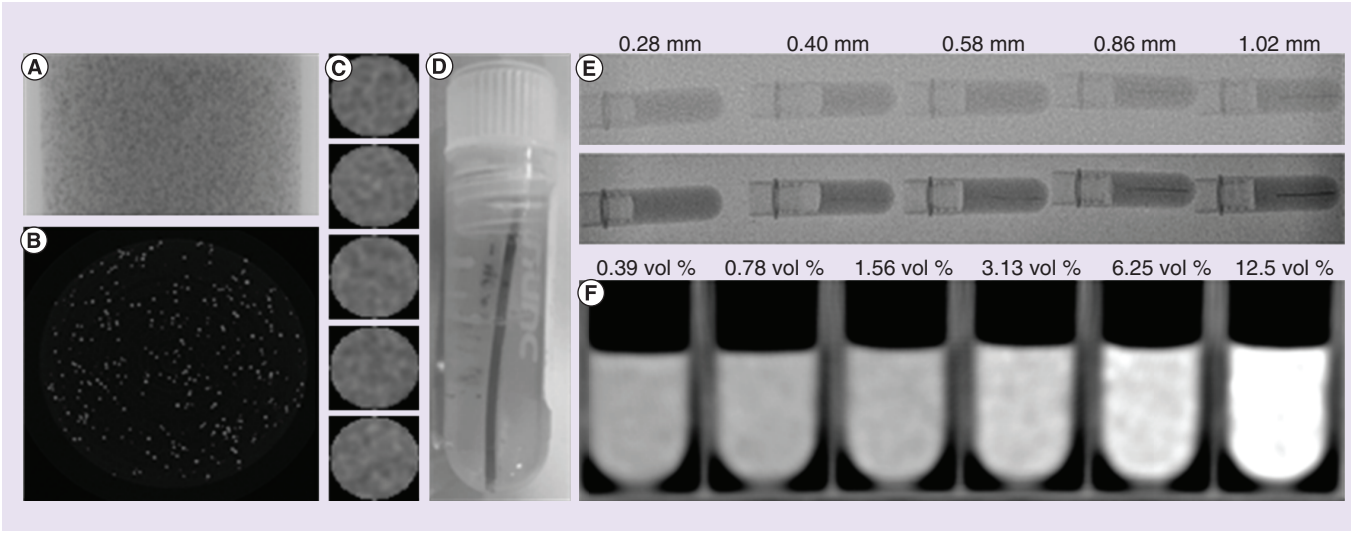

Figure 7. Micro-computed tomography of homogeneous radiopaque bead phantoms. (A) Single 2D projection; **(B)** slice through reconstructed data; and **(C)** column of individual beads (~160 μm diameter). **(D)** Photograph of a line phantom of packed beads in tubes of specified diameter and embedded in agarose. **(E)** Images of line phantoms of different line (vessel) diameters under standard fluoroscopy (upper image) and high-resolution single shot (lower image). **(F)** Computed tomography of bead suspensions in agarose of different bead concentrations in order to gauge conspicuity under computed tomography and to predict streak artefacts. Reproduced with permission from [28] © Ivyspring International (2016).

by fibrosis and tissue remodeling with complete tissue integration at day 90 with no observed chronic inflammatory or chronic immune response, indicative of a highly biocompatible material (Figure 8F) and similar to the foreign body response observed for DC Bead [88].

In a study of vessel penetration potential, DC Bead LUMI (40–90 and 70–150 μm) was compared with three other commercially available microspheres (Embozene™ 40, 100 μm and DC Bead*M1*® [70–150 μm]) by optical sizing, compressive modulus determination and penetration potential using an established 2D plate model [89]. DC Bead LUMI products had much higher compressive moduli, yet comparative penetration behavior in the plate model to the similarly sized commercial counterparts. This paralleled the observations from an *in vivo* rabbit kidney embolization model in which the same microsphere distribution patterns were obtained for the similar sized products. These results confirm that the increased stiffness of DC Bead LUMI does not measurably affect its depth of penetration within blood vessels in this model, rather the size of the microspheres being the key determinant once a threshold compressive modulus is attained.

DC Bead LUMI drug loading & the potential for future DEB dosimetry

DC Bead LUMI is composed of the same starting materials as DC Bead, and it was hypothesized that this would mean retention of its drug-loading capabilities. The existence of more hydrophobic component (and solid content) in the structure means that while the beads remain able to load the same recommended maximum doses of 37.5 mg/ml doxorubicin and 50 mg/ml of irinotecan, the loading process is slightly slower, requiring more frequent agitation than DC Bead®, and the elution profile is slower on a size-for-size basis (although *in vitro* release rates have been shown to fall within the elution envelope obtained for the smallest [70–150 μm] and largest [500–700 μm] DC Bead sizes that have both demonstrated clinical efficacy, Figure 9A) [86]. When loaded with doxorubicin, the beads turn light red in color (Figure 9B, although there is none of the associated shrinkage seen with DC Bead upon drug loading. This means there will be a full 2-ml volume of DC Bead LUMI per vial to administer at the point of treating the patient, compared with approximately 1 ml for DC Bead (Figure 9C). This fact may be partly associated with the anecdotal observation that fewer vials of DC Bead LUMI are required for similar embolization, as compared with DC Bead. One additional consequence of the increased solid content of the hydrogel matrix in DC Bead LUMI is that if so desired, doxorubicin loadings of 75 mg/ml and irinotecan loadings of 100 mg/ml can be achieved to off-set the lack of bead shrinkage.

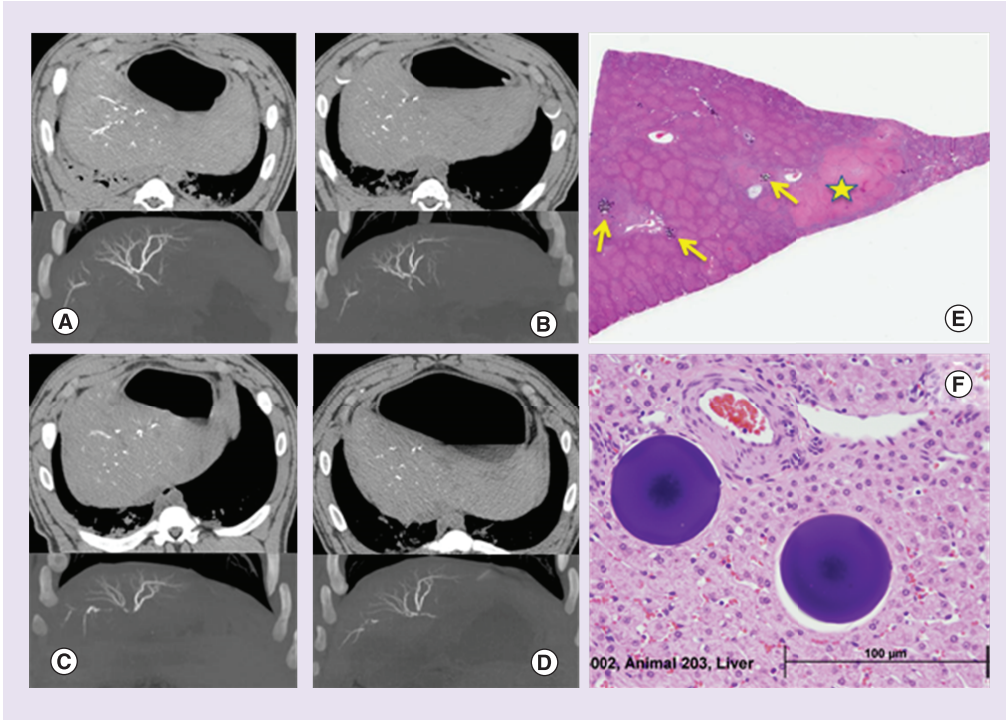

Figure 8. Imaging and pathological appearance of radiopaque beads. Longevity of the visibility of DC Bead LUMI™ observed with CT scan at 1 h, 7, 30 and 90 days postembolization (**A–D**, respectively). The top half of each image shows CT scans obtained without soluble intravenous contrast (axial plane and soft tissue windows) showing beads in the hepatic arteries. The lower half of each image shows maximum intensity projection images from CT scans obtained with soluble intravenous contrast (coronal plane and bone windows) showing more clearly the beads packed together along the lengths of hepatic arterial vessels. **(E)** Pathology of the liver at day 1 postembolization showing the presence of bead clusters (yellow arrows) and areas of focal coagulative necrosis and fibrosis (yellow star). **(F)** Integration of the beads into the remodeled hepatic tissue at day 90 with no associated long-term foreign body response.
Reproduced with permission from [87] © Elsevier (2016).

Given that we have previously demonstrated a linear correlation between doxorubicin concentration in the beads and the attenuation attributed to different concentrations of beads in suspension [24], it becomes possible to imagine the capability to visualize and localize potential drug coverage, or drug dosimetry, if one can relate imaging of bead tissue distribution to spatiotemporal diffusion of the drug around the beads. The first steps toward this goal were taken by conducting studies in which rabbit livers treated with doxorubicin-loaded DC Bead LUMI were imaged by MDCT, and a liver-specific 3D-printed mold generated from the liver image with cutting slots to allow the excised liver to be oriented as per the image and sectioned (Figure 10A). The different sections were evaluated for total radiopacity attributed to beads on MDCT, the doxorubicin extracted from each of the sections and quantified by high-pressure liquid chromatography and the correlation between the two made (Figure 10B).

This correlation between drug concentration and radiopacity was subsequently used to predict the drug levels in liver sections in a prospectively treated rabbit liver. The model was applied and predicted drug levels were compared with the actual measured levels, demonstrating excellent predictive capability (R^2 = 0.93) [90,91]. The next step in this study will be gathering an awareness of how doxorubicin is released from the beads and into the tissue over time, to allow a prediction of the drug diffusion cloud to be calculated. Furthermore, in order to understand the predictive capability of this approach to drug dosimetry, there is also a requirement to determine how well MDCT and CBCT visualize the distribution of the beads in the tissue. Therefore, comparison of DC Bead LUMI in swine liver imaged by MDCT, CBCT and micro-CT has been undertaken, and shows that both MDCT and CBCT under-report the bead distribution density as their resolution is much lower than micro-CT [92,93]. With this knowledge, allowance can be built into predictive software to allow an estimate for unseen beads present between the larger main vessels that are more easily visualized.

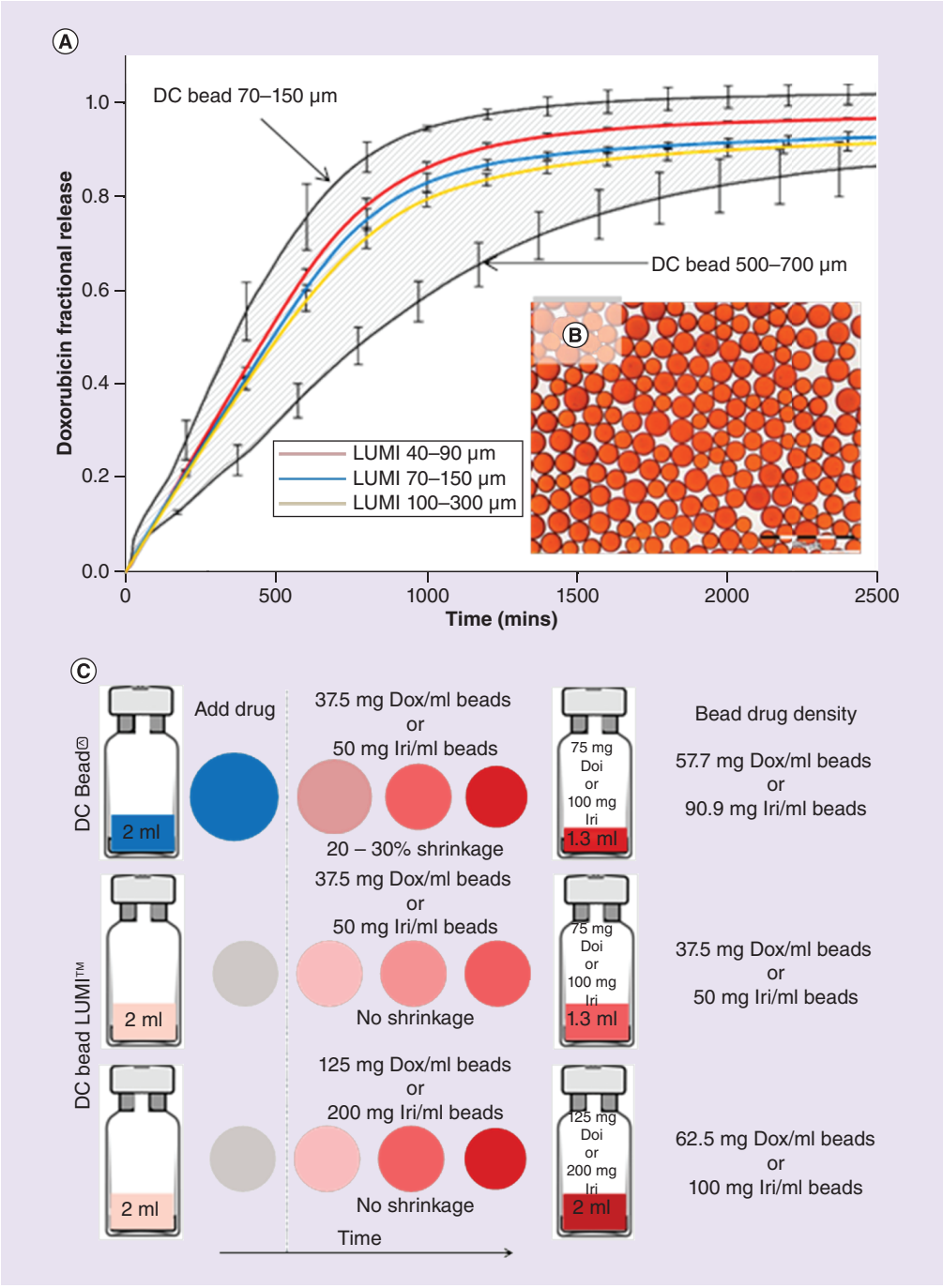

Figure 9. Effects of drug loading and elution properties of radiopaque beads. (A) *In vitro* doxorubicin release curves for the various sizes of DC Bead LUMI showing the elution profiles fall within the envelope when compared with the size extremes of DC Bead, **(B)** optical micrograph of the 70–150 µm DC Bead LUMI loaded with 37.5 mg/ml doxorubicin and **(C)** Bead dose density considerations when comparing DC Bead and DC Bead LUMI.

Clinical evaluation of DC Bead LUMI

DC Bead LUMI has not been available for clinical use for long enough to enable an extensive review of the clinical usage in patients. The first human experience was conducted at the NIH [94] under an institutional review board (IRB)-approved clinical trial. Beads were found to be easily delivered using soluble contrast with a good dilution (1 ml of beads in 18 ml contrast) and a slow delivery of no more than around 1 ml of bead suspension per minute. Delivery could be monitored during the procedure using fluoroscopy, single-shot radiography, digital subtraction

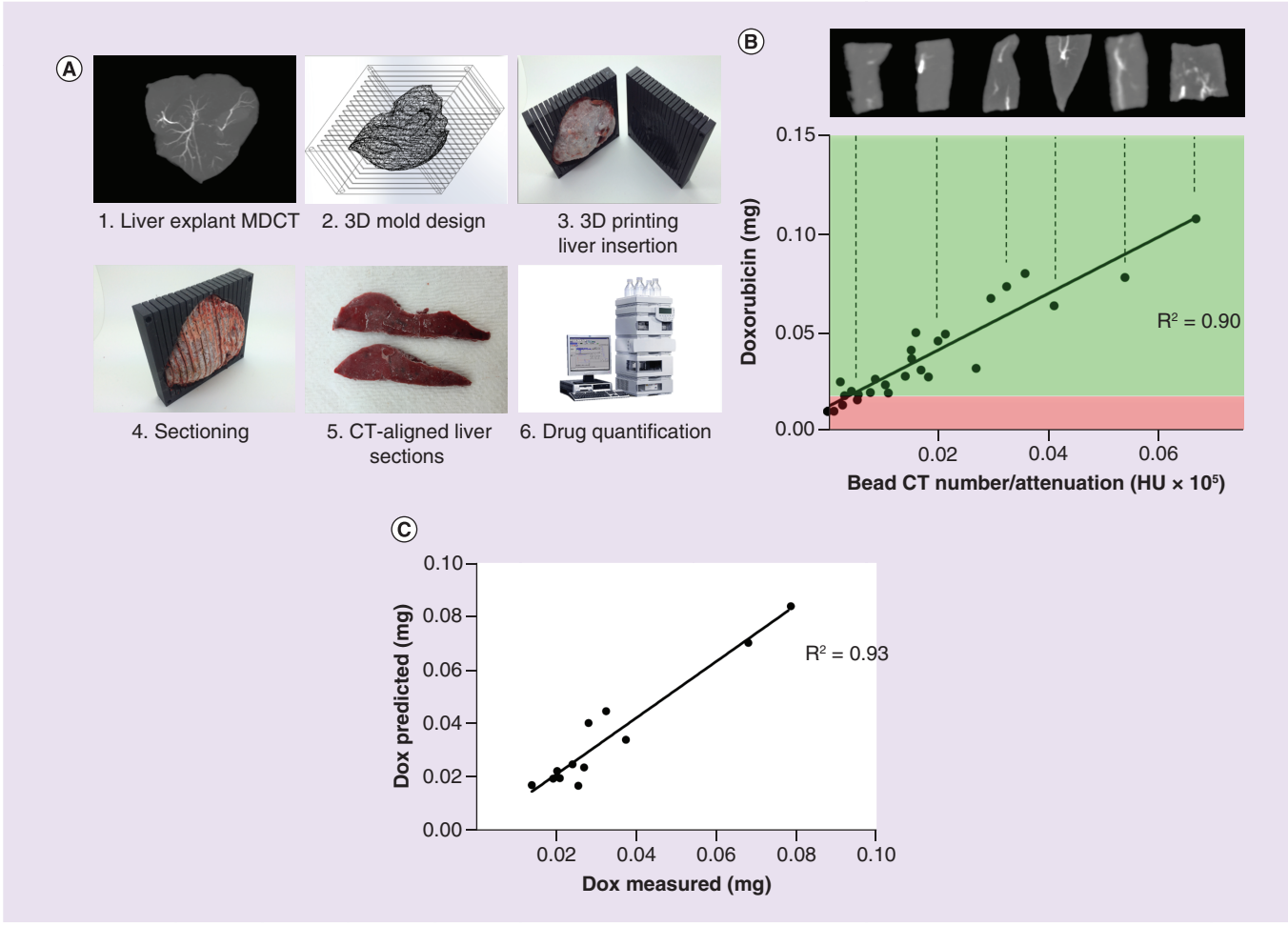

Figure 10. Study to demonstrate the correlation between radiopacity and drug concentration in tissue. (A) Process for imaging and sectioning rabbit livers treated with radiopaque drug-eluting beads; **(B)** correlation between doxorubicin levels and bead attenuation in the liver sections from three rabbits where green and red boxes demonstrate hypothetical therapeutic and subtherapeutic doses, respectively, as an illustration of potential dosimetry estimations; **(C)** evaluation of how the correlation made in **(B)** predicts drug levels based on measured radiopacity from a fourth rabbit liver.
CT: Computed tomography; MDCT: Multidetector computed tomography.

angiography, dual-phase enhanced and unenhanced CBCT and unenhanced conventional CT obtained 48 h after the procedure. As shown in dual-phase fusion CBCT and maximum intensity projection (MIP) CBCT fusion (Figure 11), intraprocedural imaging demonstrated tumor at risk for potential undertreatment, defined as paucity of radiopaque beads within a portion of the tumor that was confirmed at 48-h CT imaging, and subsequently treated with microwave ablation, after confirmation of growth in the same region. This fusion imaging is best accomplished by fusing the presoluble contrast CBCT (showing DC Bead LUMI-packed vessels alone) with an overlay of the soluble contrast-enhanced CBCT (showing perfused vessels plus vessels packed with DC Bead LUMI). This colorized subtraction or fusion image may demonstrate residual patent or unembolized vasculature, or even residual enhancing tumor (not depicted here in Figure 11).

Most recently, Aliberti *et al.* have reported on the use of DC Bead LUMI for the treatment of 44 patients with hepatocellular carcinoma (HCC) and monitored safety and bead distribution 1 h post-TACE using CT scan [95]. They observed no intraprocedural complications with low adverse events (11%) that consisted of typical mild postembolization syndrome effects. They noted nontarget distribution of beads in only two cases and the physician noted that by choosing to administer the beads in a 50:50 mixture of contrast and saline instead of 100% contrast agent, they could deliver a greater volume of beads due to the lower viscosity of the mixture. Such dilution is not recommended, as it may cause microcatheter clogging by using saline dilution. Lencioni *et al.* have also reported

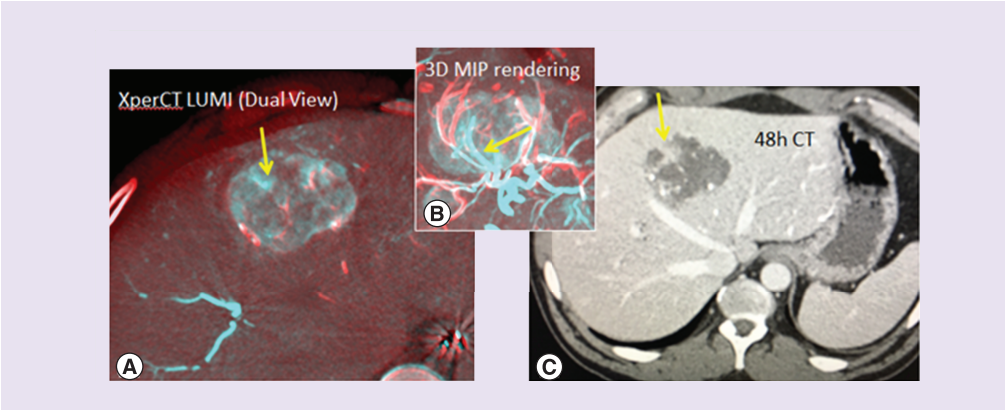

Figure 11. Images from patients treated with radiopaque beads. (A) Dual-phase fusion of cone-beam computed tomography with radiopaque beads (red) overlaid on still perfused vessels + radio-opaque beads on cone-beam computed tomography postcontrast and post-DEB-TACE (blue) showing the still perfused vascular regions without radio-opaque beads (yellow arrow shows section of one untreated artery); **(B)** 3D maximum intensity projection of the dual view of tumor vasculature (beads red, patent vessel blue) showing one artery untargeted with beads; **(C)** 48-h CT scan showing nonenhancement of most of the tumor except the undertreated region fed by the open vessel (yellow arrow).
CT: Computed tomography; DEB-TACE: Drug-eluting bead-transarterial chemoembolization.

on 48 patients with nodular, noninvasive HCC treated with 70–150 μm DC Bead LUMI loaded with 37.5 mg/ml doxorubicin [96]. High rates of both objective response (87.5%) and complete response (66.7%) were observed with only an average of 1.5 treatments per patient. There was a median time to progression of 8.5 months (median overall survival not reached at time of reporting for Child class A patients and was 19.5 months for Child class B patients). The treatment was well tolerated with a low incidence of grade 3/4 adverse events and a mild postembolization syndrome observed in a minority of patients. In a separate study, Iezzi *et al.* described the treatment of single large HCC tumors with the combination of radiofrequency ablation followed by TACE with DC Bead LUMI [97]. They noted a unique radiological sign for the prediction of successful tumor treatment that involved the visualization of DC Bead LUMI in the vessels encasing the tumor, which they nick-named the 'Hug sign'. This demonstrates that physicians are already looking into new ways in which to utilize the imageability of this novel drug-eluting embolic product for feedback during and following DEB-TACE procedures.

Indication statements

DC Bead LUMI was CE marked in March 2017 and its labeled indication is: "DC Bead LUMI can be used as an embolic agent with or without delivery of doxorubicin or irinotecan. Unloaded DC Bead LUMI is intended to be used for the embolization of nonmalignant hypervascular tumors and arteriovenous malformations (AVMs)." LC Bead LUMI was cleared by the US FDA in December 2016 and its labeled indication is: "LC Bead LUMI are intended to be used for the embolization of hypervascular tumors and arteriovenous malformations (AVMs)."

Conclusion

Interventional radiologists are accustomed to seeing a change in the radiographic appearance of treated tumors when they perform cTACE that provides a measure of confidence in treatment adequacy. However, such emulsions are not ideal surrogates for exact drug or embolic location. DEB-TACE has advantages in terms of reduced side effects because of the targeted delivery of the drug. However, the visual indication of the success of the treatment has only been indirectly inferred by the presence of trapped residual contrast by CBCT postprocedure. Radiopaque DEBs offer the ability to clearly visualize the embolic agent accumulating in the arteries during delivery, with the potential to improve efficacy by identifying tumor at risk of undertreatment and improve safety through recognition of off-target embolization. This allows the physician to tailor treatment according to the patient during the procedure, without having to wait for longer-term imaging follow-up to determine the next steps.

Future perspective

Seeing the anatomic location of DEBs may answer the question of what tissue receives drug or embolic effects. Such knowledge and procedural information may play a role in optimization, standardization and personalization of local and regional interventional oncology therapies in the future. Such standardization may facilitate clinical trial science and result in a more uniform procedure, which is otherwise quite operator variable. How and whether this new role for such information could alter practice patterns remains speculative.

What is evident following the developmental evolution of these types of imageable drug delivery embolic agents is that they are becoming more multifunctional in nature. Several examples of systems that can be imaged using a combination of different types of imaging technique (such as both x-ray and MR-based methods) are already described in the literature using 'nano-on-micro'-based approaches. Multifunctional microbeads that can be delivered via microcatheters but concentrated in the tumor by application of an external stimulus such as magnetic fields, which contain multiple drugs with complementary modes of action, that can be tracked and detected *in vivo* by multiple imaging techniques and that degrade away once the drug is released and local area has been treated, are not so much a thing of science fiction as science fact. We can expect to see such systems in clinical evaluation within the next 5 years with a view to answering the question as to whether any of these additional features can bring significant improvements to patient outcomes.

Executive summary

The time is right for imageable embolic agents

- Radiopaque embolization beads have been proposed in the literature for many years but have only recently been available commercially because of the challenges in obtaining the appropriate balance of properties to satisfy practical clinical needs.
- Advances in imaging technologies and the more routine use of cone-bead computed tomography (CBCT), for instance, enhance the value of being able to visualize the location of the radiopaque embolization beads both during and postprocedure, to ensure that the target area has good coverage, avoid undertreatment and recognize and reduce off-target distribution.

DC Bead LUMI™

- DC Bead LUMI is an inherently radiopaque drug-eluting bead (DEB) that contains iodine groups, similar to those found in soluble iodinated contrast agents, which are permanently attached to the bead structure to provide radiodensity. The product, thus far, has been evaluated predominantly in the treatment of liver malignancies and can be used bland (no drug) or loaded with doxorubicin for local treatment of hepatocellular carcinoma or irinotecan for colorectal metastases.

Finding the balance

- The bead properties have been optimized to provide the best balance between visibility and handling but the increase in bead density requires delivery of a 1:20 mixture of 1-ml bead sediment in 18 ml of pure contrast agent for ideal suspension, and delivery at a rate of 1 ml of bead suspension per minute.
- Imaging has been optimized for the 70–150 μm and 100–300 μm sizes, although 40–90 μm is under evaluation with initial reports of additional enhancements in handling and image refinement.

Paving the way for predictive drug dosimetry

- For radiopaque drug-eluting embolization beads, the measured radiopacity in tissue has been shown to correlate with the content of drug and therefore the potential exists for development of radiopaque DEB image-based dosimetry algorithms to help predict dose distribution and optimal tumor kill.

Conclusion

- Radiopaque DEBs offer the ability to clearly visualize the embolic agent accumulating in the arteries during delivery, with the potential to improve efficacy by identifying tumor at risk of undertreatment and improve safety through recognition of off-target embolization.

Disclaimer

AL Lewis, SL Willis, MR Dreher, Y Tang and K Ashrafi are employees of Biocompatibles UK Ltd, the manufacturer of DC Bead LUMI™, the product that is the subject of this review. The NIH does not in any way endorse the use of DC Bead LUMI. NIH and Biocompatibles have a Co-operative Research And Development Agreement (CRADA).

Acknowledgements

W Pritchard, J Karanian, J Esparza-Trujillo, I Bakhutashvili, O Franco and D Woods assisted in performance of certain preclinical studies. A Beck assisted with early bead preparation and evaluations. A Radaelli and M van Der Bom assisted with image processing

techniques for certain clinical cases. MM Havakuk and Q de Reuter assisted with discussion of concepts surrounding bead dosimetry. V Krishnasamy, C Garcia, V Anderson, M Cruz and J Peretti assisted with clinical trial administration.

Financial & competing interests disclosure

The corresponding author (AL Lewis) and some coauthors, (SL Willis, MR Dreher, Y Tang and K Ashrafi) are employees of Biocompatibles UK Ltd, the manufacturer of DC Bead LUMI™, the product that is the subject of this review. The authors have no other relevant affiliations or financial involvement with any organization or entity with a financial interest in or financial conflict with the subject matter or materials discussed in the manuscript apart from those disclosed.

No writing assistance was utilized in the production of this manuscript.

References

Papers of special note have been highlighted as: • of interest; •• of considerable interest

1. Golzarian J, Siskin GP, Sharafuddin M, Mumura H, Coldwell DM. Embolization tools. In: *Vascular Embolotherapy: A Comprehensive Approach, Volume 1: General Principles, Chest, Abdomen, and Great Vessels*. Springer, Berlin, Heidelberg, NY, USA, 15–33 (2006).
2. Lubarsky M, Ray C, Funaki B. Embolization agents-which one should be used when? Part 2: small-vessel embolization. *Semin. Intervent. Radiol.* 27(1), 99–104 (2010).
3. Vaidya S, Tozer KR, Chen J. An overview of embolic agents. *Semin. Intervent. Radiol.* 25(3), 204–215 (2008).
4. Dorenberg EJ, Novakovic Z, Smith HJ, Hafsahl G, Jakobsen JA. Uterine fibroid embolization can still be improved: observations on post-procedure magnetic resonance imaging. *Acta Radiol.* 46(5), 547–553 (2005).
5. Jin B, Wang D, Lewandowski RJ *et al.* Chemoembolization endpoints: effect on survival among patients with hepatocellular carcinoma. *Am. J. Roentgenol.* 196(4), 919–928 (2011).
6. Iwazawa J, Ohue S, Hashimoto N, Muramoto O, Mitani T. Survival after C-arm CT-assisted chemoembolization of unresectable hepatocellular carcinoma. *Eur. J. Radiol.* 81(12), 3985–3992 (2012).
7. Ingraham CR, Johnson GE, Nair AV, Padia SA. Nontarget embolization complicating transarterial chemoembolization in a patient with hepatocellular carcinoma. *Semin. Intervent. Radiol.* 28(2), 202–206 (2011).
8. Horak D, Metalova M, Svec F *et al.* Hydrogels in endovascular embolization. III. Radiopaque spherical particles, their preparation and properties. *Biomaterials* 8(2), 142–145 (1987).

•• **One of the earliest descriptions of the preparation of a radiopaque embolic microsphere.**

9. Thanoo BC, Jayakrishnan A. Radiopaque hydrogel microspheres. *J. Microencapsul.* 6(2), 233–244 (1989).
10. Jayakrishnan A, Thanoo BC, Rathinam K, Mohanty M. Preparation and evaluation of radiopaque hydrogel microspheres based on PHEMA/iothalamic acid and PHEMA/iopanoic acid as particulate emboli. *J. Biomed. Mater. Res.* 24, 993–1004 (1990).
11. Thanoo BC, Jayakrishnan A. Barium sulphate-loaded p(HEMA) microspheres as artificial emboli: preparation and properties. *Biomaterials* 11(7), 477–481 (1990).
12. Thanoo BC, Jayakrishnan A. Tantalum loaded silicone microspheres as particulate emboli. *J. Microencapsul.* 8(1), 95–101 (1991).
13. Thanoo BC, Sunny MC, Jayakrishnan A. Preparation and properties of barium sulphate and methyl iothalamate loaded poly(vinyl alcohol) microspheres as radiopaque particulate emboli. *J. Appl. Biomat.* 2, 67–72 (1991).
14. Horak D, Metalova M, Rypacek F. New radiopaque polyHEMA-based hydrogel particles. *J. Biomed. Mater. Res.* 34(2), 183–188 (1997).
15. Van Hooy-Corstjens CS, Saralidze K, Knetsch ML *et al.* New intrinsically radiopaque hydrophilic microspheres for embolization: synthesis and characterization. *Biomacromolecules* 9(1), 84–90 (2008).
16. Namur J, Chapot R, Pelage JP *et al.* MR imaging detection of superparamagnetic iron oxide loaded tris-acryl embolization microspheres. *J. Vasc. Interv. Radiol.* 18, 1287–1295 (2007).
17. Lee KH, Liapi E, Vossen JA *et al.* Distribution of iron oxide-containing Embosphere particles after transcatheter arterial embolization in an animal model of liver cancer: evaluation with MR imaging and implication for therapy. *J. Vasc. Interv. Radiol.* 19, 1490–1496 (2008).
18. Zielhuis SW, Seppenwoolde JH, Bakker CJ *et al.* Characterization of holmium loaded alginate microspheres for multimodality imaging and therapeutic applications. *J. Biomed. Mater. Res. A.* 82, 892–898 (2007).
19. Cilliers R, Song Y, Kohlmeir EK, Larson AC, Omary RA, Meade TJ. Modification of embolic-PVA particles with MR contrast agents. *Magn. Reson. Med.* 59, 898–902 (2008).
20. Oerlemans C, Seevinck PR, Smits ML *et al.* Holmium-Lipiodol-alginate microspheres for fluoroscopy-guided embolotherapy and multimodality imaging. *Int. J. Pharm.* 482(1-2), 47–53 (2015).
21. Wang Q, Qian K, Liu S *et al.* X-ray visible and uniform alginate microspheres loaded with in situ synthesized BaSO4 nanoparticles for in vivo transcatheter arterial embolization. *Biomacromolecules* 16, 1240–1246 (2015).
22. Chung E, Kim H, Lee G *et al.* Design of deformable chitosan microspheres loaded with superparamagnetic iron oxide nanoparticles for embolotherapy detectable by magnetic resonance imaging. *Carbohydr. Polym.* 90, 1725–1731 (2012).

23. Stampfl U, Sommer CM, Bellemann N *et al.* Multimodal visibility of a modified polyzene-F-coated spherical embolic agent for liver embolization: feasibility study in a porcine model. *J. Vasc. Interv. Radiol.* 23(9), 1225–1231, e1222 (2012).
24. Sharma KV, Dreher MR, Tang Y *et al.* Development of "imageable" beads for transcatheter embolotherapy. *J. Vasc. Interv. Radiol.* 21(6), 865–876 (2010).

• **Significant development of radiopaque beads and demonstration of real-time, intraprocedural feedback.**

25. Dreher MR, Sharma KV, Woods DL *et al.* Radiopaque drug-eluting beads for transcatheter embolotherapy: experimental study of drug penetration and coverage in swine. *J. Vasc. Interv. Radiol.* 23, 257–264, e4 (2012).
26. Tacher V, Duran R, MingDe L *et al.* Multimodality imaging of Lipiodol-loaded radiopaque microspheres in trans-arterial embolization of rabbits with VX2 liver tumors. *Radiology* 279(3), 741–753 (2016).
27. Negussie AH, Dreher MR, Gacchina JC *et al.* Synthesis and characterization of image-able polyvinyl alcohol microspheres for chemoembolization and x-ray-based imaging. *J. Mater. Sci. Mater. Med.* 26(6), 5530–5533 (2015).
28. Duran R, Ashrafi K, Sharma KV *et al.* A novel inherently radiopaque bead for intra-procedural monitoring and post-procedural evaluation of embolization to treat liver cancer. *Theranostics* 6(1), 28–39 (2016).

•• **First presentation of the utility of the DC Bead LUMI™ product in the treatment of tumors.**

29. Thanoo BC, Sunny MC, Jayakrishnan A. Tantalum-loaded polyurethane microspheres for particulate embolization: preparation and properties. *Biomaterials* 12(5), 525–528 (1991).
30. Peixoto LS, Melo PA, Nele M, Pinto JC. Expanded core/shell poly(vinyl acetate)/poly(vinyl alcohol) particles for embolization. *Macromol. Mater. Eng.* 294(8), 463–471 (2009).
31. Gacchina JC, Tang Y, Beck A *et al.* Preparation of radiopaque drug-eluting beads for transcatheter chemoembolization. *J. Vasc. Interv. Radiol.* 27(1), 117–126 (2016).
32. Saralidze K, Aldenhoff YB, Knetsch ML, Koole LH. Injectable polymeric microspheres with x-ray visibility. Preparation, properties, and potential utility as new traceable bulking agents. *Biomacromolecules* 4(3), 793–798 (2003).
33. Boelen EJ, Lewis G, Xu J, Slots T, Koole LH, Van Hooy-Corstjens CS. Evaluation of a highly-radiopaque iodine-containing acrylic bone cement for use in augmentation of vertebral compression fractures. *J. Biomed. Mater. Res. A.* 86(1), 76–88 (2008).
34. Van Hooy-Corstjens CS, Bulstra SK, Knetsch ML, Geusens P, Kuijer R, Koole LH. Biocompatibility of a new radiopaque iodine-containing acrylic bone cement. *J. Biomed. Mater. Res. B. Appl. Biomater.* 80(2), 339–344 (2007).
35. Boelen EJ, Koole LH, Van Rhijn LW, Van Hooy-Corstjens CS. Towards a functional radiopaque hydrogel for nucleus pulposus replacement. *J. Biomed. Mater. Res. B. Appl. Biomater.* 83(2), 440–450 (2007).
36. Boelen EJ, Van Hooy-Corstjens CS, Bulstra SK, Van Ooij A, Van Rhijn LW, Koole LH. Intrinsically radiopaque hydrogels for nucleus pulposus replacement. *Biomaterials* 26(33), 6674–6683 (2005).
37. Horak D, Svec F, Kalal J *et al.* Hydrogels in endovascular embolization. IV. Effect of radiopaque spherical particles on the living tissue. *Biomaterials* 9(4), 367–371 (1988).
38. Lewis AL. DC Bead™: a major development in the toolbox for the interventional oncologist. *Expert Rev. Med. Dev.* 6(4), 389–400 (2009).
39. Lewis AL, Gonzalez MV, Lloyd AW *et al.* DC bead: *in vitro* characterization of a drug-delivery device for transarterial chemoembolization. *J. Vasc. Interv. Radiol.* 17(2 Pt 1), 335–342 (2006).
40. Liapi E, Lee KH, Georgiades CC, Hong K, Geschwind JF. Drug-eluting particles for interventional pharmacology. *Tech. Vasc. Interv. Radiol.* 10(4), 261–269 (2007).
41. Malagari K. Drug-eluting particles in the treatment of HCC: chemoembolization with doxorubicin-loaded DC Bead. *Expert Rev. Anticancer Ther.* 8(10), 1643–1650 (2008).
42. Nicolini A, Crespi S, Martinetti L. Drug delivery embolization systems: a physician's perspective. *Expert Opin. Drug Deliv.* 8(8), 1071–1084 (2011).
43. Kim HC. Role of C-arm cone-beam CT in chemoembolization for hepatocellular carcinoma. *Korean J. Radiol.* 16(1), 114–124 (2015).
44. Minami Y, Murakami T, Kitano M, Sakurai T, Nishida N, Kudo M. Cone-beam CT angiography for hepatocellular carcinoma: current status. *Dig. Dis.* 33(6), 759–764 (2015).
45. Tacher V, Lin M, Bhagat N *et al.* Dual-phase cone-beam computed tomography to see, reach, and treat hepatocellular carcinoma during drug-eluting beads transarterial chemo-embolization. *J. Vis. Exp.* (82), 50795 (2013).
46. Bannerman D, Wan W. Multifunctional microbeads for drug delivery in TACE. *Expert Opin. Drug Deliv.* 13(9), 1289–1300 (2016).
47. Van Elk M, Ozbakir B, Barten-Rijbroek AD *et al.* Alginate microspheres containing temperature sensitive liposomes (TSL) for MR-guided embolization and triggered release of doxorubicin. *PLoS ONE* 10(11), e0141626 (2015).
48. Kim DH, Li W, Chen J *et al.* Multimodal imaging of nanocomposite microspheres for transcatheter intra-arterial drug delivery to liver tumors. *Sci. Rep.* 6, 29653 (2016).
49. Huang K, Zhou Q, Wang R, Cheng D, Ma Y. Doxorubicin-eluting beads versus conventional transarterial chemoembolization for the treatment of hepatocellular carcinoma. *J. Gastroenterol. Hepatol.* 29(5), 920–925 (2014).

50. Kloeckner R, Weinmann A, Prinz F *et al.* Conventional transarterial chemoembolization versus drug-eluting bead transarterial chemoembolization for the treatment of hepatocellular carcinoma. *BMC Cancer* 15, 465 (2015).

51. Lencioni R. Chemoembolization for hepatocellular carcinoma. *Semin. Oncol.* 39(4), 503–509 (2012).

52. Lencioni R. Management of hepatocellular carcinoma with transarterial chemoembolization in the era of systemic targeted therapy. *Crit. Rev. Oncol. Hematol.* 83(2), 216–224 (2012).

53. Ni JY, Xu LF, Wang WD, Sun HL, Chen YT. Conventional transarterial chemoembolization vs microsphere embolization in hepatocellular carcinoma: a meta-analysis. *World J. Gastroenterol.* 20(45), 17206–17217 (2014).

54. Song MJ, Park CH, Kim JD *et al.* Drug-eluting bead loaded with doxorubicin versus conventional Lipiodol-based transarterial chemoembolization in the treatment of hepatocellular carcinoma: a case–control study of Asian patients. *Eur. J. Gastroenterol. Hepatol.* 23(6), 521–527 (2011).

55. Dubbelboer IR, Lilienberg E, Ahnfelt E *et al.* Treatment of intermediate stage hepatocellular carcinoma: a review of intrahepatic doxorubicin drug-delivery systems. *Ther. Deliv.* 5(4), 447–466 (2014).

56. Giunchedi P, Maestri M, Gavini E, Dionigi P, Rassu G. Transarterial chemoembolization of hepatocellular carcinoma – agents and drugs: an overview. Part 2. *Expert Opin. Drug Deliv.* 10(6), 799–810 (2013).

57. Giunchedi P, Maestri M, Gavini E, Dionigi P, Rassu G. Transarterial chemoembolization of hepatocellular carcinoma – agents and drugs: an overview. Part 1. *Expert Opin. Drug Deliv.* 10(5), 679–690 (2013).

58. Lilienberg E, Dubbelboer IR, Karalli A *et al. In vivo* drug delivery performance of Lipiodol-based emulsion or drug-eluting beads in patients with hepatocellular carcinoma. *Mol. Pharm.* 14(2), 448–458 (2017).

59. Lilienberg E, Ebeling Barbier C, Nyman R *et al.* Investigation of hepatobiliary disposition of doxorubicin following intrahepatic delivery of different dosage forms. *Mol. Pharm.* 11(1), 131–144 (2014).

60. Idee JM, Guiu B. Use of Lipiodol as a drug-delivery system for transcatheter arterial chemoembolization of hepatocellular carcinoma: a review. *Crit. Rev. Oncol. Hematol.* 88(3), 530–549 (2013).

61. Lewis AL, Dreher MR. Locoregional drug delivery using image-guided intra-arterial drug eluting bead therapy. *J. Control. Rel.* 161(2), 338–350 (2012).

62. Liapi E, Geschwind JF. Transcatheter arterial chemoembolization for liver cancer: is it time to distinguish conventional from drug-eluting chemoembolization? *Cardiovasc. Intervent. Radiol.* 34(1), 37–49 (2011).

63. Hong K, Khwaja A, Liapi E, Torbenson MS, Georgiades CS, Geschwind JF. New intra-arterial drug delivery system for the treatment of liver cancer: preclinical assessment in a rabbit model of liver cancer. *Clin. Cancer Res.* 12(8), 2563–2567 (2006).

64. Poon RTP, Tso WK, Pang RWC *et al.* A Phase I/II trial of chemoembolization for hepatocellular carcinoma using a novel intra-arterial drug-eluting bead. *Clin. Gastroenterol. Hepatol.* 5(9), 1100–1108 (2007).

65. Varela M, Real MI, Burrel M *et al.* Chemoembolization of hepatocellular carcinoma with drug eluting beads: efficacy and doxorubicin pharmacokinetics. *J. Hepatol.* 46(3), 474–481 (2007).

• **Clinical study that demonstrates effectiveness of drug-eluting bead-transarterial chemoembolization and favorable pharmacokinetic profile.**

66. Lammer J, Malagari K, Vogl T *et al.* Prospective randomized study of doxorubicin-eluting-bead embolization in the treatment of hepatocellular carcinoma: results of the PRECISION V study. *Cardiovasc. Intervent. Radiol.* 33(1), 41–52 (2010).

•• **Important randomized clinical study of safety and efficacy of drug-eluting bead-transarterial chemoembolization versus conventional oil-based transarterial chemoembolization.**

67. Recchia F, Passalacqua G, Filauri P *et al.* Chemoembolization of unresectable hepatocellular carcinoma: decreased toxicity with slow-release doxorubicineluting beads compared with Lipiodol. *Oncol. Rep.* 27(5), 1377–1383 (2012).

68. Kan Z, Mccuskey PA, Wright KC, Wallace S. Role of Kupffer cells in iodized oil embolization. *Invest. Radiol.* 29(11), 990–993 (1994).

69. Kan Z, Sato M, Ivancev K *et al.* Distribution and effect of iodized poppyseed oil in the liver after hepatic artery embolization: experimental study in several animal species. *Radiology* 186(3), 861–866 (1993).

70. Okayasu I, Hatakeyama S, Yoshida T *et al.* Selective and persistent deposition and gradual drainage of iodized oil, Lipiodol in the hepatocellular carcinoma after injection into the feeding hepatic artery. *Am. J. Clin. Pathol.* 90(5), 536–544 (1988).

71. Kanematsu T, Matsumata T, Furuta T *et al.* Lipiodol drug targeting in the treatment of primary hepatocellular carcinoma. *Hepatogastroenterology* 37(5), 442–444 (1990).

72. Gaba RC, Baumgarten S, Omene BO *et al.* Ethiodized oil uptake does not predict doxorubicin drug delivery after chemoembolization in VX2 liver tumors. *J. Vasc. Interv. Radiol.* 23(2), 265–273 (2012).

• **Important work that demonstrates oil uptake in tumors treated by conventional oil-based transarterial chemoembolization does not correlate with drug location.**

73. Kim DY, Ryu HJ, Choi JY *et al.* Radiological response predicts survival following transarterial chemoembolisation in patients with unresectable hepatocellular carcinoma. *Aliment. Pharmacol. Ther.* 35(11), 1343–1350 (2012).

74. El Khaddari S, Gaudin JL, Abidi H, Picaud G, Rode A, Souquet JC. Chemoembolization in hepatocellular carcinoma: multivariate analysis of survival prognostic factors after the first session. *Gastroenterologie Clinique et Biologique* 26(8–9), 728–734 (2002).

75. Li J, Shao W, Song J, Shi C, Chen H, Cong N. The therapeutic effect of transcatheter arterial thromboembolization of hepatocellular carcinoma as for residual viable tumors related to lipoidal density areas and detected by (18)F-FDG PET/CT and CT. *Hell. J. Nucl. Med.* 16(1), 64–65 (2013).
76. Cho YZ, Park SY, Choi EH *et al.* The usefulness of contrast-enhanced ultrasonography in the early detection of hepatocellular carcinoma viability after transarterial chemoembolization: pilot study. *Clin. Mol. Hepatol.* 21(2), 165–174 (2015).
77. Wang Z, Lin M, Lesage D *et al.* Three-dimensional evaluation of Lipiodol retention in HCC after chemoembolization: a quantitative comparison between CBCT and MDCT. *Acad. Radiol.* 21(3), 393–399 (2014).
78. Hu J, Maybody M, Cao G *et al.* Lipiodol retention pattern assessed by cone beam computed tomography during conventional transarterial chemoembolization of hepatocellular carcinoma: accuracy and correlation with response. *Cancer Imaging* 16(1), 32 (2016).
79. Wang Z, Chen R, Duran R *et al.* Intraprocedural 3D quantification of Lipiodol deposition on cone-beam CT predicts tumor response after transarterial chemoembolization in patients with hepatocellular carcinoma. *Cardiovasc. Intervent. Radiol.* 38(6), 1548–1556 (2015).
80. Johnson CG, Sharma KV, Levy EB *et al.* Microvascular perfusion changes following transarterial hepatic tumor embolization. *J. Vasc. Interv. Radiol.* 27(1), 133–141, e133 (2016).
81. Lencioni R, Baere T, Burrel M *et al.* Transcatheter treatment of hepatocellular carcinoma with doxorubicin-loaded DC bead (DEBDOX): technical recommendations. *Cardiovasc. Intervent. Radiol.* 35(5), 980–985 (2012).
82. Suk Oh J, Jong Chun H, Gil Choi B, Giu Lee H. Transarterial chemoembolization with drug-eluting beads in hepatocellular carcinoma: usefulness of contrast saturation features on cone-beam computed tomography imaging for predicting short-term tumor response. *J. Vasc. Interv. Radiol.* 24(4), 483–489 (2013).
83. Golowa YS, Cynamon J, Reinus JF *et al.* Value of noncontrast CT immediately after transarterial chemoembolization of hepatocellular carcinoma with drug-eluting beads. *J. Vasc. Interv. Radiol.* 23(8), 1031–1035 (2012).
84. Wang SJ, Lin WY, Lui WY, Chen MN, Tsai ZT, Ting G. Hepatic artery injection of Yttrium-90-Lipiodol: biodistribution in rats with hepatoma. *J. Nucl. Med.* 37(2), 332–335 (1996).
85. Emans PJ, Saralidze K, Knetsch ML, Gijbels MJ, Kuijer R, Koole LH. Development of new injectable bulking agents: biocompatibility of radiopaque polymeric microspheres studied in a mouse model. *J. Biomed. Mater. Res. A.* 73(4), 430–436 (2005).
86. Ashrafi K, Tang Y, Britton H *et al.* Characterization of a novel intrinsically radiopaque drug-eluting bead for image-guided therapy: DC bead LUMI. *J. Control. Rel.* 250, 36–47 (2017).

• **First description of the drug delivery capabilitie of DC Bead LUMI.**

87. Sharma KV, Bascal Z, Kilpatrick H *et al.* Long-term biocompatibility, imaging appearance and tissue effects associated with delivery of a novel radiopaque embolization bead for image-guided therapy. *Biomaterials* 103, 293–304 (2016).

• **Demonstration that the radiopacity from DC Bead LUMI is long-lived.**

88. Lewis AL, Taylor RR, Hall B, Gonzalez MV, Willis SL, Stratford PW. Pharmacokinetic and safety study of doxorubicin-eluting beads in a porcine model of hepatic arterial embolization. *J. Vasc. Interv. Radiol.* 17(8), 1335–1343 (2006).
89. Caine M, Zhang X, Hill M *et al.* Comparison of microsphere penetration with LC bead LUMI versus other commercial microspheres. *J. Mech. Behav. Biomed. Mater.* 78, 46–55 (2017).
90. Mikhail A, Levy EB, Krishnasamy VP *et al.* Mapping drug dose distribution with conventional IR imaging following hepatic DEBTACE with drug-eluting radiopaque beads (DEROB). *J. Vasc. Interv. Radiol.* 27(3 Suppl.), S126–S127 (2016).
91. Mikhail AS, Pritchard WF, Negussie AH *et al*. Mapping drug dose distribution on CT with radiopaque drug-eluting beads for DEB-TACE in a rabbit tumor model. *Radiology* (2018) (In press).
92. Thompson J, Pritchard W, Bakhutashvili I *et al.* Assessment of radiopaque bead volume and distribution following hepatic TACE in swine: CBCT and microCT. *J. Vasc. Interv. Radiol.* 28(2S), S9 (2017).
93. Thompson JG, Van Der Sterren W, Bakhutashvili I *et al.* Distribution and detection of radiopaque beads after hepatic transarterial embolization in swine: cone-beam CT versus microCT. *J. Vasc. Interv. Radiol.* 29(4), 568–574 (2018).
94. Levy EB, Krishnasamy VP, Lewis AL *et al.* First human experience with directly image-able iodinated embolization microbeads. *Cardiovasc. Intervent. Radiol.* 39(8), 1177–1186 (2016).

•• **First human experience with DC Bead LUMI and demonstration of the utility of radipaque beads for identifying areas at risk of undertreatment.**

95. Aliberti C, Carandina R, Sarti D *et al.* Transarterial chemoembolization with DC Bead LUMI radiopaque beads for primary liver cancer treatment: preliminary experience. *Future Oncol.* 13(25), 2243–2252 (2017).

• **First European safety and efficacy study in hepatocellular carcinoma patients for DC Bead LUMI.**

96. Lencioni R, Fraud T, Doshi M, Venkat S, Echenique A, Narayanan G. Transarterial chemoembolization of hepatocellular carcinoma with a novel radiopaque drug eluting bead. *J. Clin. Oncol.* 36(Suppl. 4S), Abstract 366 (2018).
97. Iezzi R, Pompili M, Annicchiarico EB *et al.* 'Hug sign': a new radiological sign of intraprocedural success after combined treatment for hepatocellular carcinoma. *Hepat. Oncol.* 4(3), 69–73 (2017).